Microstructure and Electronic Structure of Transparent Ferromagnetic ZnO−Spinel Iron Oxide Composite Films

Tsutomu Shinagawa,*,† Masanobu Izaki,† Haruyuki Inui,‡ Kuniaki Murase,‡ and Yasuhiro Awakura‡

Department of Electronic Materials, Osaka Municipal Technical Research Institute, 1-6-50 Morinomiya, Joto-ku, Osaka 536-8553, Japan, and Department of Material Science and Engineering, Kyoto University, Kyoto 606-8501, Japan

Received October 20, 2005. Revised Manuscript Received December 1, 2005

Transparent ZnO films with ferromagnetic spinel iron oxide particles (Fe 9.5 atom %) were prepared on glass substrates by a novel chemical process followed by heat treatment at 773 K under vacuum. The chemical process involved (i) ZnO deposition from an aqueous solution and (ii) the introduction of iron atoms into the ZnO in another aqueous solution containing iron ions. The microstructure and electronic structure of the films were characterized in detail by using transmission electron microscope (TEM) analyses, X-ray absorption fine structure (XAFS), and soft X-ray magnetic circular dichroism (SXMCD). TEM observation revealed that the film had a heterogranular structure composed of iron oxide particles of 20 nm in diameter embedded in a wurtzite ZnO matrix. Both the Fe K-edge XAFS and Fe $L_{2,3}$-edge SXMCD measurements using synchrotron radiation techniques indicated that the iron oxide particles were zinc-substituted magnetite ($Zn_xFe_{3-x}O_4$, $x \approx 0.5$) with a cubic spinel structure, which is the origin of ferromagnetism. Negative magnetoresistance of −0.35% was found at room temperature as well as an n-type semiconducting feature.

Introduction

Magnetic materials with a heterogranular structure have been intensively investigated because they exhibit magnetoresistance (MR) and soft magnetic properties.[1] In particular, the semiconductor−ferromagnet composite material with a heterogranular structure, where nanosized magnetic particles are embedded in a semiconductor matrix, is a key material to realize spintronics devices because of its anomalous spin-dependent effects.[2] The GaAs−MnAs heterogranular system has been prepared by heat treatment of molecular beam epitaxy (MBE) grown Mn-doped GaAs,[3] and various III−V GaAs-based semiconductor−ferromagnet systems have been reported,[4] where negative and/or positive MR were observed mainly at low temperature.

On the other hand, few heterogranular systems based on II−VI semiconductors have been reported except for the ZnO−Co composite materials reported recently.[5] II−VI ZnO is widely used in industrial applications such as transparent conductive films, varistors, chemical gas sensors, and surface acoustic wave devices, due to its various useful properties of high visible transparency, semiconductivity, piezoelectricity, fluorescence, and photoconductivity. Recently, ZnO has received much attention as a host-semiconductor of diluted magnetic semiconductors with room-temperature ferromagnetism[6] and as a UV light emitting material because of its wide band gap energy (3.3 eV) and high exciton binding energy (60 meV).[7]

* Corresponding author. E-mail: tshina@omtri.city.osaka.jp.
† Osaka Municipal Technical Research Institute.
‡ Kyoto University.

(1) (a) Berkowitz, A.; Mitchell, J. R.; Carey, M. J.; Young, A. P.; Zhang, S.; Spada, F. E.; Parker, F. T.; Hutten, A.; Thomas, G. *Phys. Rev. Lett.* **1992**, *68*, 3745. (b) Xiao, J. Q.; Jiang, J. S.; Chien, C. L. *Phys. Rev. Lett.* **1992**, *68*, 3749.

(2) (a) Prinz, G. *Science* **1990**, *250*, 1092. (b) Shi, J.; Kikkawa, J. M.; Proksch, R.; Schäffer, T.; Awshalom, D. D.; Medeiros-Ribeiro, G.; Petroff, P. M. *Nature* **1995**, *377*, 707. (c) Moreno, M.; Jenichen, B.; Kaganer, V.; Braun, W.; Trampert, A.; Däweritz, L.; Ploog, K. H. *Phys. Rev. B* **2003**, *67*, 235206.

(3) De Boeck, J.; Oesterholt, R.; Van Esch, A.; Bender, H.; Bruynseraede, C.; Van Hoof, C.; Borghs, G. *Appl. Phys. Lett.* **1996**, *68*, 2744.

(4) For (In,Ga)As−Fe, see: (a) McInturff, D. T.; Harmon, E. S.; Chang, J. C. P.; Pekarek, T. M.; Woodall, J. M. *Appl. Phys. Lett.* **1996**, *69*, 1885. (b) Pekarek, T. M.; Crooker, B. C.; Li, S.; McElfresh, M.; Chang, J. C. P.; McInturff, D.; Harmon, E. S.; Melloch, M. R.; Woodall, J. M. *J. Appl. Phys.* **1997**, *81*, 4869. For GaAs−MnAs, see: (c) Wellmann, P. J.; Garcia, J. M.; Feng, J.-L.; Petroff, P. M. *Appl. Phys. Lett.* **1997**, *71*, 2532. (d) Akinaga, H.; De Boeck, J.; Borghs, G.; Miyanishi, S.; Asamitsu, A. Van Roy, W.; Tomioka, Y.; Kuo, L. H. *Appl. Phys. Lett.* **1998**, *72*, 3368. (e) Wellman, P. J.; Garcia, J. M.; Feng, J. L.; Petroff, P. M. *Appl. Phys. Lett*. **1998**, *73*, 387. (i) Hayashi, T.; Hashimoto, Y.; Katsumoto, S.; Iye, Y. *Appl. Phys. Lett.* **2001**, *78*, 1691. (j) Shimizu, H.; Tanaka, M. *J. Appl. Phys.* **2001**, *89*, 7281. (k) Yuldashev, Sh. U.; Shon, Y.; Kwon, Y. H.; Fu, D. J.; Kim, D. Y.; Kim, H. J.; Kang, T. W. *J. Appl. Phys.* **2001**, *90*, 3004. For GaAs−ErAs, see: (f) Schmidt, D. R.; Petukhov, A. G.; Foygel, M.; Ibbetson, J. P.; Allen, S. J. *Phys. Rev. B* **1999**, *82*, 823. For GaAs−MnSb, see: (g) Akinaga, H.; Miyanishi, S.; Tanaka, K.; Van Roy, W.; Onodera, K. *Appl. Phys. Lett.* **2000**, *76*, 97. For GaAs−Fe, see: (h) Haneda, S.; Munekata, H.; Takatani, Y.; Koshihara, S. *J. Appl. Phys.* **2000**, *87*, 6445. For (GaMnAs)−MnAs, see: (l) Ye, S.; Klar, P. J.; Hartmann, Th.; Heimbrodt, W.; Lampalzer, M.; Nau, S.; Torunski, T.; Stolz, W.; Kurz, T.; K. von Nidda, H.-A.; Loidl, A. *Appl. Phys. Lett.* **2003**, *83*, 3927.

(5) Pakhomov, A. B.; Roberts, B. K.; Tuan, A.; Shutthanandan, V.; McCready, D.; Thevuthasan, S.; Chambers, S. A.; Krishnan, K. M. *J. Appl. Phys.* **2004**, *95*, 7393.

(6) Theoretical, see: (a) Dietl, T.; Ohno, H.; Matsukura, F.; Cibert, J.; Ferrand, D. *Science* **2000**, *287*, 1019. (b) Katayama-Yoshida, H.; Sato, K. *Physica B* **2003**, *327*, 337. Experimental, see: (c) Ueda, K.; Tabata, H.; Kawai, T. *Appl. Phys. Lett.* **2001**, *79*, 988. (d) Han, S.-J.; Song, J. W.; Yang, C.-H.; Park, S. H.; Park, J.-H.; Jeong, Y. H. *Appl. Phys. Lett.* **2002**, *81*, 4212. (e) Pakhomov, A. B.; Roberts, B. K.; Krishnan, K. M. *Appl. Phys. Lett.* **2003**, *38*, 2877. (f) Sharma, P.; Gupta, A.; Rao, K. V.; Owens, F. J.; Sharma, R.; Ahuja, R.; Guillen, J. M. O.; Johansson, B.; Gehring, G. A. *Nat. Mater.* **2003**, *2*, 673.

10.1021/cm052309t CCC: $33.50
Published on Web 01/06/2006

We have reported a chemical method to provide a transparent ferromagnetic composite film based on a II−VI ZnO semiconductor. The composite film was composed of a spinel iron oxide phase and ZnO matrix. Such a composite material with the combination of a crystalline oxide semiconductor and a crystalline oxide ferromagnet is quite novel because of the complexity of crystal growth. The synthesis of the ZnO−spinel iron oxide composite film was achieved by a simple three-step process:[8] (i) chemical bath deposition of ZnO from an aqueous solution,[9] (ii) chemical bath introduction of Fe into the ZnO deposit from another aqueous solution,[10] and (iii) heat treatment under vacuum. The chemical method, called a "soft-solution process", has several advantages over gas-phase deposition processes as follows: (i) the thickness and morphology of the film can be controlled by electrochemical parameters; (ii) relatively uniform films can be obtained on substrates even with complicated shapes or microfabricated patterns; (iii) the manufacturing cost including apparatus and raw materials can be kept reasonably low; and (iv) the technique used is less hazardous and more friendly to the environment.

The spin-dependent effects of the ZnO−spinel iron oxide composite film strongly depend on the stoichiometry of the spinel iron oxide phases, unlike composite systems with metal particles, and also on how ferromagnets were embedded in the semiconductor matrix. This is because the ferromagnetic property of spinel iron oxides such as Fe_3O_4 (magnetite) and MFe_2O_4 (transition-metal-substituted ferrite) is based on ferrimagnetism originating in the antiferromagnetic superexchange interaction among metal atoms through oxygen atoms, whereas the ferromagnetism of metals such as Fe and Co results from the exchange interaction among 3d electrons.[11] The magnetic moment of spinel iron oxide compounds, therefore, changes significantly depending on the stoichiometry and atomic arrangement in the lattice. Precise identification of spinel iron oxides is, however, difficult even for the bulk sample because $Fe^{II,III}$ cations with two kinds of oxidation states can occupy two coordination sites in a spinel lattice. In the present paper, we show detailed structural characteristics including morphology and stoichiometry of spinel iron oxide particles embedded in the ZnO matrix prepared by the chemical bath reactions. Furthermore, optical, electrical, and magnetic properties arising from the unique ZnO−spinel iron oxide film are demonstrated.

The structural characterization was performed by transmission electron microscope (TEM) observation, X-ray absorption fine structure (XAFS), and soft X-ray magnetic circular dichroism (SXMCD) measurements. Both the XAFS and SXMCD methods are discussed based upon the X-ray absorption spectra (XAS) of an element focused in a specimen at energies near and above its absorption edge. XAFS including X-ray absorption near-edge structure (XANES) and extended X-ray absorption fine structure (EXAFS) provides information about the oxidation state and the local structure of the element in the specimen on a short-range order scale. Radial distribution functions (RDFs) calculated from EXAFS give some averaged information about parameters of the local structure such as coordination number of the element and its distance from the nearest neighbors.[12] Therefore, XAFS is a powerful technique to determine the oxidation state[13] and the cation distribution[14] of spinel iron oxide compounds with a rather complex lattice. On the other hand, SXMCD using circularly polarized X-rays is sensitive to the electron and magnetic structures of an X-ray-absorbing magnetic element.[15] The MCD spectrum is the difference in intensity between the XAS recorded both with right and left circularly polarized X-rays under a magnetic field. Since the magnetic property of 3d transition-metal compounds mainly depends on their d valence electrons, intensive studies have been reported on MCD at $L_{2,3}$-edge corresponding to excitation (2p → 3d). MCD signals can be obtained clearly even for nanosized magnetic particles by using a synchrotron light source and are very effective to identify them.[16]

Experimental Section

General Procedures. Chemical bath depositions of films from aqueous solutions were carried out under ambient atmosphere using reagent grade chemicals and deionized water purified by a Mill-RX12 Plus system. A Corning glass (no. 1737) or a synthesized

(7) (a) Bagnall, D. M.; Chen, Y. F.; Zhu, Z.; Yao, T.; Koyama, S.; Shen, M. Y.; Goto, T. *Appl. Phys. Lett.* **1997**, *70*, 2230. (b) Segawa, Y.; Ohtomo, A.; Kawasaki, M.; Shono, T.; Hasegawa, T.; Koshihara, S.; Koinuma, H. *Phys. Status Solidi A* **1997**, *202*, 669. (c) Huang, M. H.; Mao, S.; Feick, H.; Yan, H.; Wu, Y.; Kind, H.; Weber, E.; Russo, R.; Yang, P. *Science* **2001**, *292*, 1897. (d) Izaki, M.; Watase, S.; Takahashi, H. *Adv. Mater.* **2003**, *15*, 2000.

(8) Shinagawa, T.; Izaki, M.; Matsumura, Y.; Murase, K.; Awakura, Y. *Electrochem. Solid-State Lett.* **2004**, *7*, G235.

(9) (a) Izaki, M.; Omi, T. *J. Electrochem. Soc.* **1997**, *144*, L3. (b) Izaki, M.; Katayama, J. *J. Electrochem. Soc.* **2000**, *147*, 210.

(10) (a) Izaki, M.; Takino, A.; Shinagawa, T.; Tasaka, A. *Trans. Mater. Res. Soc. Jpn.* **2003**, *28*, 337. (b) Shinagawa, T.; Izaki, M.; Inui, H.; Murase, K.; Awakura, Y. *J. Electrochem. Soc.* **2005**, *152*, G736.

(11) Chikazumi, S. *Physics of Ferromagnetism*, 2nd ed.; Oxford University Press: New York, 1997.

(12) For examples, see: (a) Koningsberger, D. C.; Prins, R. *X-ray Absorption: Principles, Applications, Techniques of EXAFS*; Wiley & Sons: New York, 1988. (b) Teo, B. K. *EXAFS: Basic Principles and Data Analysis*; Springer-Verlag: Berlin, 1986. (c) Iwasawa, Y. *X-ray Absorption Fine Structure for Catalysis and Surfaces*; World Scientific: Singapore, 1996.

(13) (a) Sasaki, S. *Rev. Sci. Instrum.* **1995**, *66*, 1573. (b) Matsumoto, K.; Saito, F.; Toyoda, T.; Ohkubo, K.; Yamawaki, K.; Mori, T.; Hirano, K.; Tanaka, M.; Sasaki, S. *Jpn. J. Appl. Phys.* **2000**, *39*, 6089.

(14) (a) Jeyadevan, B.; Tohji, K.; Nakatsuka, K. *J. Appl. Phys.* **1994**, *76*, 6325. (b) Harris, V. G.; Koon, N. C.; Wiliams, C. M.; Zhang, Q.; Abe, M.; Kirkland, J. P.; McKeown, D. A. *IEEE Trans. Magn.* **1995**, *31*, 3473. (c) Harris, V. G.; Koon, N. C.; Williams, C. M.; Zhang, Q.; Abe, M.; Kirkland, J. P. *Appl. Phys. Lett.* **1996**, *68*, 2082. (d) Harris, V. G.; Koon, N. C.; Williams, C. M.; Zhang, Q. Abe, M. *J. Appl. Phys.* **1996**, *79*, 4561. (e) Carpenter, E. E.; O'Connor, C. J.; Harris, V. G. *J. Appl. Phys.* **1999**, *85*, 5175. (f) Chinnasamy, C. N.; Narayanasamy, A.; Ponpandian, N.; Chattopandhyay, K.; Shinoda, K.; Jeyadevan, B. Tohji, K.; Nakatsuka, K.; Furubayashi, T.; Nakatani, I. *Phys. Rev. B* **2001**, *63*, 184108. (g) Calvin, S.; Carpenter, E. E.; Ravel, B.; Harris, V. G.; Morrison, S. A. *Phys. Rev. B* **2002**, *66*, 224405.

(15) For examples, see: (a) Schütz, G.; Wagner, W.; Wilhelm, W.; Kienle, P.; Zeller, R.; Frahm, R.; Materlik, G. *Phys. Rev. Lett.* **1987**, *58*, 73. (b) Chen, C. T.; Sette, F.; Ma, Y.; Modesti, S. *Phys. Rev. B* **1990**, *42*, 7262. (c) Thole, B. T.; Carra, P.; Sette, F.; van der Laan, G. *Phys. Rev. Lett.* **1992**, *68*, 1943. (d) Ebert, H.; Schütz, G. *Spin−Orbit-Influenced Spectroscopies of Magnetic Solids*; Springer: Berlin, 1996.

(16) For examples, see: (a) Okabayashi, J.; Mizuguchi, M.; Oshima, M.; Shimizu, H.; Tanaka, M.; Yuri, M.; Chen, C. T. *Appl. Phys. Lett.* **2003**, *83*, 5485. (b) Park, J.; Lee, E.; Hwang, N.-M.; Kang, M.; Kim, S. C.; Hwang, Y.; Park, J.-G.; Noh, H.-J.; Kim, J.-Y.; Park, J.-H.; Hyeon, T. *Angew. Chem., Int. Ed.* **2005**, *44*, 2872. (c) Lee, Y.; Lee, J.; Bae, C. J.; Park, J.-G.; Noh, H.-J.; Park, J.-H.; Hyeon, T. *Adv. Funct. Mater.* **2005**, *15*, 503.

quartz glass was used as a substrate. Prior to chemical deposition, the substrate was rinsed with acetone and deionized water and was catalyzed using an industrially employed three-step Sn/Ag/Pd activation process (C. Uyemura Co., Ltd., S-10X, MSA-27, and A-10X). This activation process was carried out by sequentially immersing the substrate into these three aqueous solutions for 1 min, resulting in the substrate becoming entirely covered with Pd catalytic particles at high density.

Preparation of ZnO−Spinel Films. $Zn(NO_3)_2 \cdot 6H_2O$ and dimethylamine borane (DMAB) were dissolved in the deionized water to prepare an aqueous 0.03 M $Zn(NO_3)_2$−0.01 M DMAB solution with pH 5.6. The resulting solution was heated to 333 K with stirring. The glass substrate catalyzed as mentioned above was immersed into the solution for 30 min without stirring to deposit ZnO. The film obtained was rinsed with deionized water and then dried under ambient atmosphere.

$Fe(NO_3)_3 \cdot 9H_2O$ and DMAB were dissolved in the deionized water to prepare an aqueous 0.01 M $Fe(NO_3)_3$−0.03 M DMAB solution. The pH of the resulting solution was 2.4. The solution was stirred and heated to 323 K. The as-deposited ZnO film was immersed into the solution for 20 min without stirring to incorporate Fe into the ZnO film. The resultant film was rinsed with deionized water, dried under ambient atmosphere, and finally heat treated at 773 K for 1 h in a vacuum furnace at around 5×10^{-4} Pa.

Characterization of Films. The thickness of films was measured at three different positions by a surface-roughness analyzer (Tokyo Seimitsu Co., Ltd., Surfcom 1500A), and the three measured values were averaged. The contents of Fe and Zn in the ZnO−spinel iron oxide film were determined with inductively coupled plasma atomic emission spectroscopy (ICP-AES, Seiko Instruments SPS-1500VR). The sample for the ICP analysis was prepared by dissolving the film into a diluted HCl aqueous solution. X-ray diffraction (XRD) patterns were measured using a Rigaku RINT 2500 system with monochromated Cu Kα radiation (40 kV, 200 mA). Microstructures in the plan-view geometry of the film were observed with a transmission electron microscope (TEM, JEM-2000FX) operated at an accelerating voltage of 200 kV. Selected area electron diffraction (SAED) patterns were taken from areas 750 nm in diameter. Inspection of local compositions was carried out with a high-resolution scanning TEM (JEM-2010F) equipped with a nanoprobe energy-dispersive spectrometer (EDS) with an electron probe of 0.7 nm in diameter and operated at 200 kV. The TEM samples in the plan-view geometry were prepared as follows. The quartz glass substrate of 100 μm in thickness with the ZnO−spinel iron oxide film was cut into a disk 3.0 mm in diameter using slurry drilling. The disk was dimpled to below 30 μm in thickness, and then ion-milling with 5 keV Ar ions was performed from the quartz side using a precision ion-polishing system (Gatan model 691). X-ray absorption fine structure (XAFS) at the Fe and Zn K-edges and soft X-ray magnetic circular dichroism (SXMCD) at the Fe $L_{2,3}$-edge were measured for the ZnO−spinel iron oxide films at the beam lines BL01B1 and BL25SU, respectively, of the Japan Synchrotron Radiation Research Institute (JASRI), SPring-8. Furthermore, XAFS at the Fe and/or Zn K-edges were measured using the following high-purity powdered oxides for reference (Kojundo Chemical Lab Co., Ltd.): Fe_3O_4 (magnetite), $Zn_xFe_{3-x}O_4$ (Zn-substituted magnetite, $x = 0.4$, 0.6, and 0.8), $ZnFe_2O_4$ (zinc ferrite), α-Fe_2O_3 (hematite), FeO (wüstite), and ZnO (zinc oxide). XAFS data for the films were recorded at a low incident angle of about 2° with a Lytle-type detector, and a transmission mode was employed for the reference oxides. Fourier transformation was performed on k^3-weighted EXAFS spectra using a REX2000 program supplied by Rigaku to calculate pseudo-radial distribution functions (RDFs). The MCD spectra were recorded by means of a total electron yield method switching light helicity (right/left circularly polarized X-ray) at 1 Hz under the condition of ultrahigh vacuum. A magnetic field of 14 kOe (1 kOe = 0.1 T) was applied perpendicular to the film plane using a Nd−Fe−B magnetic circuit. Optical transmittance spectra for glass substrates coated with films on both the faces were recorded with a spectrophotometer (Shimadzu UV-3150C) referenced to air. Electrical properties including electrical resistivity and carrier type were evaluated with a van der Pauw method using a Hall effect measuring system (Toyo Technica, Resitest 8320). Evaluation of magnetization was carried out using a vibrating sample magnetometer (VSM, Riken Denshi Co., Ltd., BHV-50H) referenced to a standard Ni plate, and the diamagnetic contribution of the glass substrate was subtracted. Magnetic field dependence of magnetoresistance was recorded with the VSM at room temperature, where a magnetic field was applied parallel to both the film plane and an applied current.

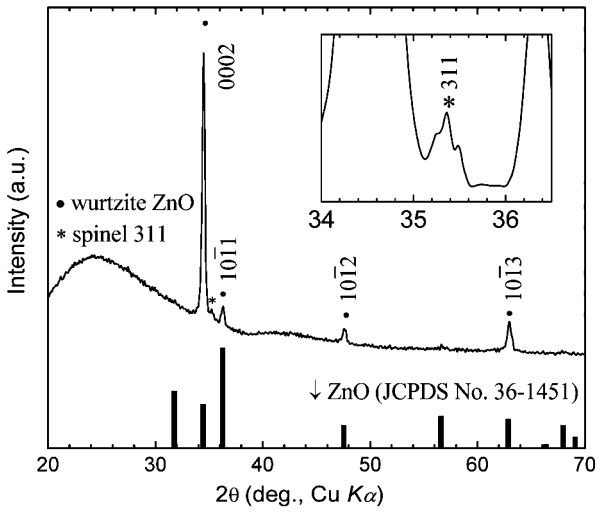

Figure 1. XRD pattern for the ZnO−spinel film prepared on a glass substrate, and the expanded view of a peak assigned to spinel 311 reflection.

Results and Discussion

The thickness of the ZnO−spinel iron oxide film did not change before and after the heat treatment and was determined to be 240 nm. From the absolute contents of Fe and Zn in the film by the ICP analyses and the weight, the composition of the film was estimated to be 9.5 atom % Fe, 40.5 atom % Zn, and 50% O, and the film is abbreviated as "ZnO−spinel" in the present paper.

XRD Pattern for the ZnO−Spinel Film. Figure 1 shows the X-ray diffraction (XRD) pattern for the ZnO−spinel film. In addition to reflections of wurtzite ZnO (JCPDS no. 36-1451) with a ⟨0001⟩ preferred growth orientation, a weak peak was observed at 35.36° in 2θ, located between 35.42° due to the 311 reflection of Fe_3O_4 (JCPDS no. 19-0629) and 35.26° due to the 311 reflection of $ZnFe_2O_4$ (JCPDS no. 22-1012) with cubic spinel structures. Although this suggested that the film was a mixture of ZnO and spinel iron oxide, detailed analysis was difficult because of the trace reflection intensity.

Microstructure of the ZnO−Spinel Film. Figure 2a shows a plan-view TEM image of the ZnO−spinel film. As indicated by the arrows, small particles about 20 nm in diameter were observed inside the large grains of 100 nm in size and at their boundaries. Figure 2b shows the selected

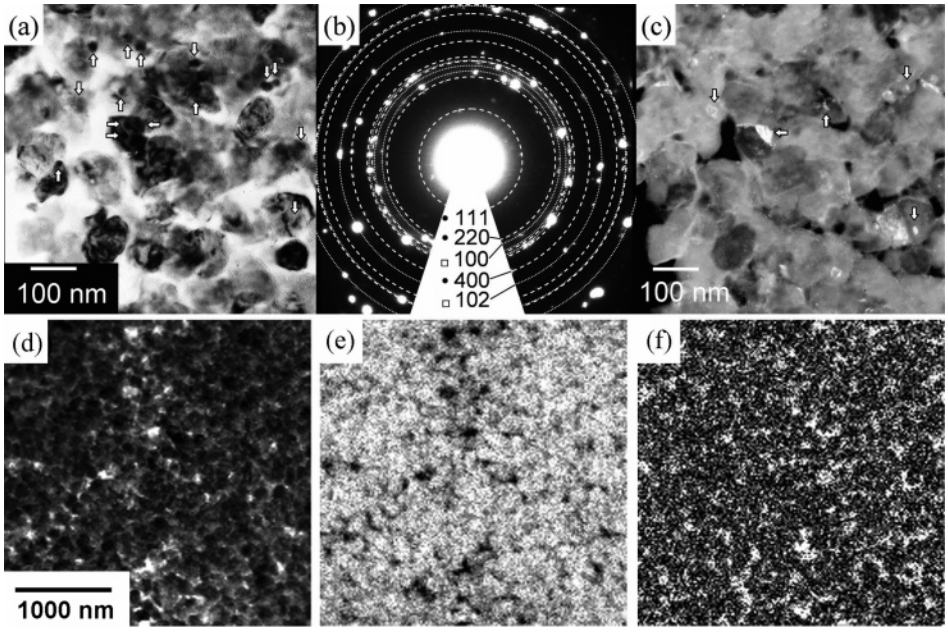

Figure 2. (a) Plan-view TEM image of the ZnO−spinel film prepared on a glass substrate, (b) corresponding SAED pattern, and (c) dark-field image taken with spinel 111 reflection. The SAED was taken from an area with a diameter of 750 nm, and the indices correspond to those from spinel Fe_3O_4 or $ZnFe_2O_4$ (●, JCPDS no. 19-0629, 22-1012) and wurtzite ZnO (□, JCPDS no. 36-1451). (d) Plan-view TEM image and (e, f) elemental distribution maps of the film; (e) Zn map and (f) Fe map. The maps were made by EDS with an electron probe of 0.7 nm in diameter.

area electron diffraction (SAED) pattern from an area 750 nm in diameter. Almost all the diffraction spots observed were consistently assigned either to wurtzite ZnO (dotted line) or spinel iron oxide (dashed line). Larger grains corresponded to wurtzite ZnO and smaller ones to spinel iron oxide, since bright regions in dark-field images (Figure 2c) taken with the spinel 111 reflection exclusively agreed with the small grains observed in Figure 2a. Parts 2d−f of Figure 2 show a plan-view TEM image and elemental distribution maps of Zn and Fe in the corresponding area and were taken with a nanoprobe EDS. Zn atoms were dispersed homogeneously inside ZnO grains, while Fe atoms were observed as the form of particles which were dispersed homogeneously in the ZnO matrix.

EXAFS Oscillation Spectra for the ZnO−Spinel Film. Here, we used a low-angle X-ray incident method at an incident angle of about 2° to give clearer EXAFS oscillations than those recorded at the conventional incident angle of 45° already reported,[8] allowing precise comparison with standard references of high-purity iron oxides. Figure 3 represents k^3-weighted EXAFS spectra, $k^3\chi(k)$ at the Fe and Zn K-edges for the ZnO−spinel film together with those for reference oxides. The reference oxides include FeO (NaCl-type structure), Fe_3O_4 (cubic spinel structure), α-Fe_2O_3 (α-Al_2O_3-type structure), $ZnFe_2O_4$ (cubic spinel structure), and ZnO (wurtzite structure). These spectra provide detailed information on the averaged atomic environment around an X-ray-absorbing element.[12] The EXAFS spectrum at the Fe K-edge for the ZnO−spinel film showed clear oscillation up to the high-k region, and its peak positions were in good agreement with those of the spinel iron oxides, Fe_3O_4 and $ZnFe_2O_4$, over the region examined. This indicates that the averaged local structure around the Fe atoms in the film definitely corresponds to a spinel structure.

On the other hand, the oscillation of the EXAFS spectrum at the Zn K-edge for the film is almost the same as that for reference ZnO, and the presence of the $ZnFe_2O_4$ in the film was not recognized.

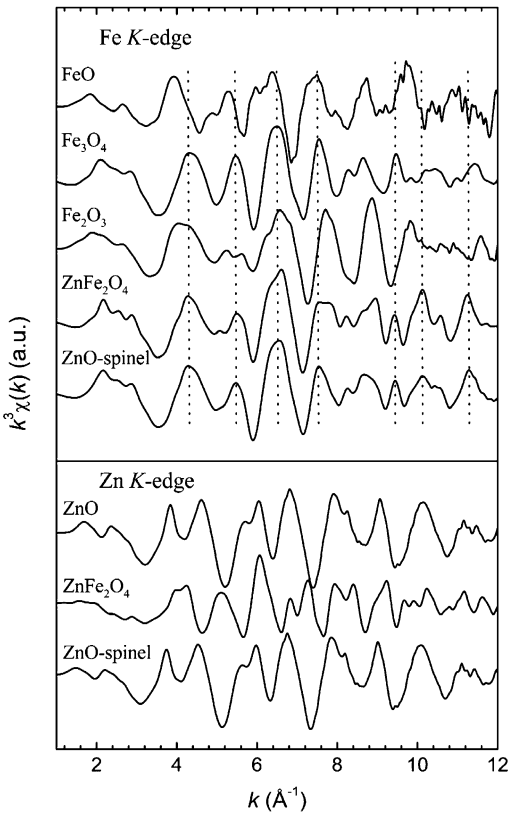

Figure 3. Normalized k^3-weighted EXAFS spectra, $k^3\chi(k)$, at the Fe K-edge (top) and Zn K-edge (bottom) for the ZnO−spinel film prepared on a glass substrate and the reference oxides FeO, Fe_3O_4, α-Fe_2O_3, $ZnFe_2O_4$, and ZnO.

Valence States of Fe in the ZnO−Spinel Film. Figure 4 shows the normalized X-ray absorption near-edge structure (XANES) spectra at the Fe K-edge for the ZnO−spinel film and reference iron oxides. XANES is the region of the X-ray absorption spectrum within ∼50 eV of the absorption edge

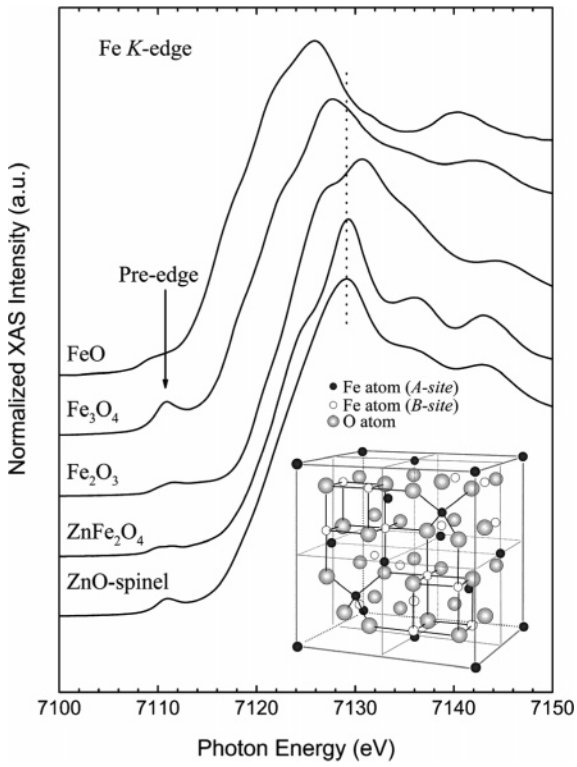

Figure 4. Normalized XANES spectra at the Fe K-edge for the ZnO−spinel film prepared on a glass substrate and the reference oxides FeO, Fe_3O_4, α-Fe_2O_3, and $ZnFe_2O_4$. The inset shows the crystal structure of spinel Fe_3O_4. The O atom is on the fcc lattice. One out of eight of the tetrahedral sites (A-sites) and half of the octahedral sites (B-sites) are occupied by Fe atoms, yielding 32 O, 8 Fe(A), and 16 Fe(B) per unit cell.

including the preedge. XANES provides information about the oxidation state affected by the local coordination environment around an X-ray-absorbing element.[12] A preedge peak characteristic to Fe_3O_4 was observed at around 7111 eV on the spectrum for the ZnO−spinel film. Fe_3O_4, expressed as $Fe^{III}_A[Fe^{II},Fe^{III}]_BO_4$, is a well-known ferrimagnetic material, in which half of the Fe^{III} cations occupy tetrahedral sites (A-sites) and the residual Fe^{III} and Fe^{II} cations occupy octahedral sites (B-sites) in a cubic inverse spinel lattice as shown in an inset of Figure 4.[11] This kind of definite preedge can be detected in the case of Fe^{III} cations occupying tetrahedral sites (Fe^{III}(A)) in a spinel lattice,[13b] suggesting that the ZnO−spinel film includes some Fe^{III}(A) cations in a spinel lattice.

Furthermore, it is known that the position of the main peak at the Fe K-edge for iron oxides with octahedral coordination changes depending on the oxidation states of the Fe atoms.[13a] The peak for FeO with only Fe^{II} cations occupying the octahedral sites was located at 7125.9 eV, which was lower by 5.0 eV than that of 7130.9 eV for α-Fe_2O_3 with only Fe^{III} cations occupying the octahedral sites. Therefore, the peak for Fe_3O_4 containing both Fe^{II} and Fe^{III} cations in octahedral sites is located at 7127.8 eV between those for FeO and α-Fe_2O_3. In the case of $ZnFe_2O_4$, expressed as $Zn^{II}_A[Fe^{III}_2]_BO_4$, with a cubic spinel structure, Zn^{II} cations normally occupy A-sites because of their strong preference to tetrahedral coordination, and two equivalent Fe^{III} cations occupy the residual B-sites.[11] Therefore, the main peak for $ZnFe_2O_4$ at the Fe K-edge appeared at a photon energy of 7129.2 eV, higher than that of Fe_3O_4. The difference in peak position

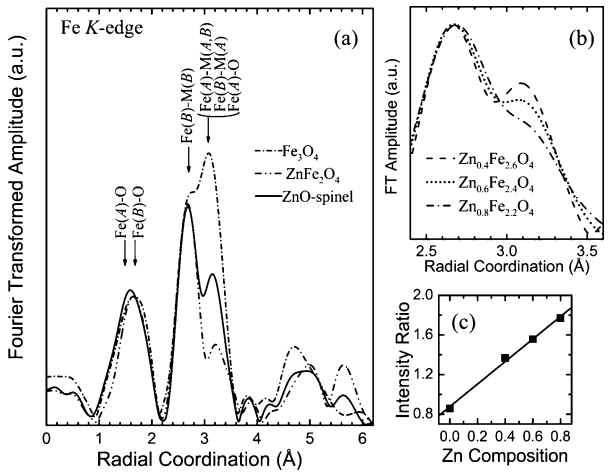

Figure 5. (a) Normalized Fourier transformed amplitude (RDF) at the Fe K-edge for the ZnO−spinel film prepared on a glass substrate (solid) and the reference oxides of Fe_3O_4 (dash dot) and $ZnFe_2O_4$ (dash dot dot). (b) Expanded view of the second peak of normalized RDF at the Fe K-edge for a series of $Zn_xFe_{3-x}O_4$ ($x = 0.4, 0.6, 0.8$). Data have not been corrected for electron phase shifts. (c) Relationship between the intensity ratio of low-*r* peak at around 2.7 to the high-*r* peak at around 3.1 Å on the Fe K-edge RDF (low-*r*/high-*r*) for the reference iron oxides, $Zn_xFe_{3-x}O_4$, *x* ($0 \le x \le 0.8$) and Zn composition.

between α-Fe_2O_3 and $ZnFe_2O_4$ probably depends on their lattice structures. The photon energy of 7129.0 eV at the Fe K-edge peak for the ZnO−spinel film approximately coincided with that of $ZnFe_2O_4$, but the profile of the main peak was broadened toward the lower energy side. The findings suggest that most of the Fe cations in the film were in the Fe^{III} state while some Fe^{II} were also included there.

RDF of the ZnO−Spinel Film. Pseudo-radial distribution functions (RDFs) calculated by Fourier transformation of EXAFS spectra provide detailed information on the local crystallographic parameters around an X-ray-absorbing element such as its coordination numbers and the distance to neighbor shells from it.[12] Figure 5a shows the Fe K-edge RDF for the ZnO−spinel film together with those for the reference iron oxides of Fe_3O_4 and $ZnFe_2O_4$. These RDFs were normalized in the peak height corresponding to the first nearest shell. The first peak at around 1.6 Å for Fe_3O_4, expressed as $Fe^{III}_A[Fe^{II},Fe^{III}]_BO_4$, convolutes three peaks due to Fe^{III}(A)−O (low-*r*) and $Fe^{II,III}$(B)−O (high-*r*) coordination, where the distance of the Fe^{III}(B)−O coordination is slightly shorter than that of the Fe^{II}(B)−O. The second doublet peak is composed of Fe(B)−Fe(B) coordination (ca. 2.7 Å) and some coordination (ca. 3.1 Å) mainly of Fe(A)−Fe(A,B), Fe(B)−Fe(A), and Fe(A)−O.[14] The separate appearance of the Fe(B)−Fe(B) coordination in the second doublet peak makes it a unique fingerprint in a ferrite system.

An Fe^{III} cation in $ZnFe_2O_4$ ($Zn^{II}_A[Fe^{III}_2]_BO_4$) has only Fe^{III}-(B)−O, Fe^{III}(B)−Fe^{III}(B), and Fe^{III}(B)−Zn^{II}(A) coordination because all A-sites are occupied by Zn^{II} cations as mentioned above. Therefore, the second doublet peak on the Fe K-edge RDF for $ZnFe_2O_4$ is composed of a rather sharp peak (ca. 2.7 Å) due to the Fe^{III}(B)−Fe^{III}(B) coordination with almost the same intensity as that of Fe_3O_4 and a weak hybridized one containing the Fe^{III}(B)−O and Fe^{III}(B)−Zn^{II}(A) coordination (ca. 3.1 Å). It is known that since $ZnFe_2O_4$ does not possess strong superexchange interaction between Fe(B) and Fe(A) cations through an oxygen atom, i.e., of

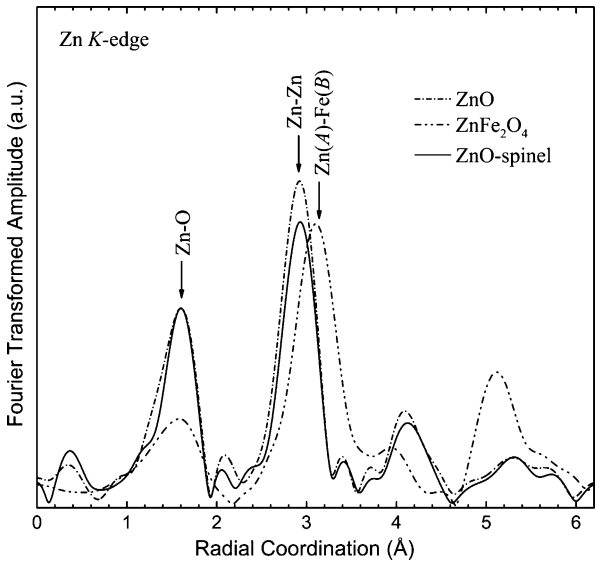

Figure 6. Normalized Fourier transformed amplitude (RDF) at the Zn K-edge for the ZnO−spinel film prepared on a glass substrate (solid) and the reference oxides of ZnO (dash dot) and $ZnFe_2O_4$ (dash dot dot). Data have not been corrected for electron phase shifts.

Fe(B)−O−Fe(A), an antiferromagnetic behavior with a very low Néel temperature of 9.5 K due to the weak interaction of Fe(B)−O−Fe(B) is observed.[11]

It is clear from Figure 5a that the low-*r* peak at around 2.7 Å in the second doublet peak of the ZnO−spinel film was almost equivalent to that of $ZnFe_2O_4$, revealing that the spinel iron oxide in the film contains stoichiometric Fe cations in its B-sites. Furthermore, the intensity of the high-*r* hybridized one (ca. 3.1 Å) for the film lay between those for Fe_3O_4 and $ZnFe_2O_4$, demonstrating that there are some Zn cations in A-sites of the spinel iron oxide in the film. From these results, the spinel iron oxide particles in the film were identified as Zn-substituted Fe_3O_4, i.e., $Zn_xFe_{3-x}O_4$. The compound $Zn_xFe_{3-x}O_4$ is known to exhibit ferrimagnetism with a magnetic moment which is superior to that of Fe_3O_4 up to the value of $x = 0.7$.[11] Figure 5b shows the expanded view of the second doublet peak on RDF at the Fe K-edge for a series of $Zn_xFe_{3-x}O_4$ ($x = 0.4, 0.6, 0.8$), which was single-phase Zn-substituted Fe_3O_4 with a cubic spinel structure, expressed as $[Zn^{II}_x,Fe^{III}_{1-x}]_A[Fe^{II}_{1-x},Fe^{III}_{1+x}]_BO_4$. The low-*r* peaks from the Fe(B)−Fe(B) coordination exhibited constant intensity independent of *x* value, while the high-*r* peaks decreased in their intensity depending on the *x* value, i.e., the number of Zn cations occupying the A-site. Figure 5c shows the relationship between the intensity ratio of the low-*r* peak to high-*r* peak and the Zn composition for the reference iron oxides of $Zn_xFe_{3-x}O_4$ ($x = 0.4, 0.6, 0.8$) and Fe_3O_4, representing a linear relationship between them. The peak intensity ratio of the ZnO−spinel film was 1.44. Thus, the composition of the spinel iron oxide in the film was estimated to have $x = 0.5$ in the $Zn_xFe_{3-x}O_4$.

Figure 6 shows normalized RDFs at the Zn K-edge for the ZnO−spinel film and the reference oxides of ZnO and $ZnFe_2O_4$. The film showed RDF similar to that for ZnO as seen in EXAFS spectra (Figure 3), and no sign of Zn cations in the iron oxide particles was observed probably because of their considerably smaller amount.

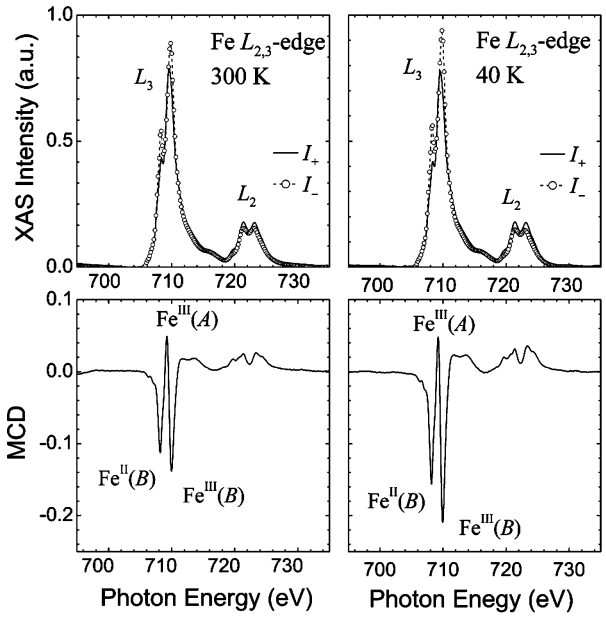

Figure 7. Normalized XAS (top) and MCD (bottom) spectra at the Fe $L_{2,3}$-edge measured at 40 and 300 K for the ZnO−spinel film prepared on a glass substrate. The curves I_+ and I_- represent the XAS intensity for the right and left circularly polarized X-rays, respectively, and MCD is the difference ($I_+ - I_-$) between these XAS at each energy.

MCD for the ZnO−Spinel Film. The Fe $L_{2,3}$-edge X-ray absorption spectra (XAS) and corresponding magnetic circular dichroism (MCD) spectrum for the ZnO−spinel film measured at 40 and 300 K are shown in Figure 7. It was observed at 40 K that the intensity of each MCD peak become large; a trend similar to that of the temperature dependence of the magnetization measured by the VSM.[8] XAS and MCD spectra recorded for the film exhibited features characteristic to ferrites, of which all the peaks were already assigned.[17] The contribution of Fe^{II}(B) and Fe^{III}(B) cations with majority spin was observed in the L_3-edge region of the MCD spectra as negative peaks at energies of 708.16 and 709.96 eV, while that of the Fe^{III}(A) cations with minority spin was observed as a positive peak at an energy of 709.22 eV. On the other hand, two peaks with positive intensity were observed in the L_2-edge region. The peak intensities of Fe^{II}(B) and Fe^{III}(A) cations in the MCD spectra were, however, weak as compared with those already reported for stoichiometric Fe_3O_4,[18] indicating that the composition of the spinel iron oxide in the film was different from that of Fe_3O_4; some Fe^{II}(B) and Fe^{III}(A) cations were deficient. This is because the peak intensity and position of the MCD peaks reflect directly the amount of spin-polarized species active in the ferromagnetism and their chemical and coordination states based on the electronic structure, respectively. This deficiency of Fe^{II}(B) and Fe^{III}(A) cations is in agreement with the result derived from the EXAFS analysis, i.e., Zn-incorporated Fe_3O_4, $[Zn^{II}_x,Fe^{III}_{1-x}]_A[Fe^{II}_{1-x},Fe^{III}_{1+x}]_BO_4$, revealing definitely that the ferromagnetic behavior of the film originates in the $Zn_xFe_{3-x}O_4$ ($x \approx 0.5$) particles with the superexchange interaction of Fe(A)−O−Fe(B).

(17) Kuiper, P.; Searle, B. G.; Duda, L.-C.; Wolf, R. M.; van der Zaag, P. J. *J. Electron Spectrosc. Relat. Phenom.* **1997**, *86*, 107.
(18) Morrall, P.; Schedin, F.; Case, G. S.; Thomas, M. F.; Dudzik, E.; van der Laan, G.; Thornton, G. *Phys. Rev. B* **2003**, *67*, 214408.

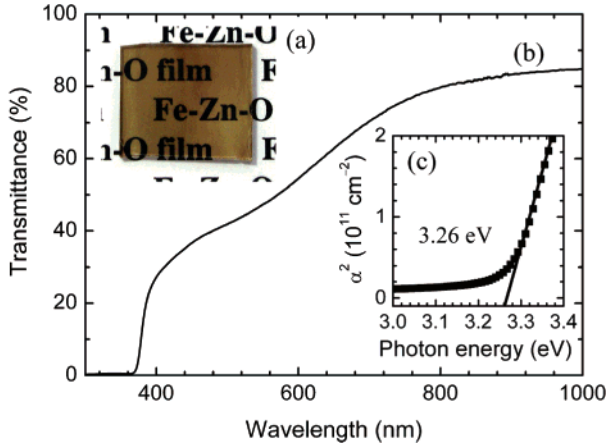

Figure 8. (a) Photograph and (b) transmittance spectrum of the ZnO−spinel film prepared on a glass substrate. The spectrum was referenced to air. The inset (c) is the dependence of α^2 (α, absorption coefficient) on photon energy for the film.

Optical and Electrical Properties of the ZnO−Spinel Film. Figure 8 shows an optical transmittance spectrum and the appearance of a glass substrate coated on both sides with the ZnO−spinel film. The dark-brown colored film adhered uniformly over the entire substrate surface and showed transparency from 40% to 80% in the visible light regions. Since ZnO film containing no Fe was colorless with higher transparency, the difference in the appearance between the ZnO−spinel and ZnO films originates in the spinel iron oxide particles. The band gap energy for the ZnO−spinel film was estimated to be 3.26 eV by extrapolating the linear part of the relationship between α^2 and the photon energy to $\alpha^2 = 0$, where α is the absorption coefficient, as shown in an inset of Figure 8. This energy band gap is a characteristic value for ZnO with a wurtzite structure.

The electrical resistivity of the ZnO−spinel film was 2.6 Ω cm, and the carrier type was identified as n-type by Hall effects, indicating that the film is an n-type semiconducting film. In addition, the carrier concentration and mobility were 2.4×10^{18} cm^{-3} and 0.82 cm^2 V^{-1} s^{-1}, respectively. On the other hand, the electrical resistivity, carrier concentration, and mobility for the heat-treated ZnO film were 0.52 Ω cm, 3.8×10^{18} cm^{-3}, and 3.2 cm^2 V^{-1} s^{-1}, respectively. The difference in mobility between the two films suggests that the spinel iron oxide particles in the ZnO−spinel film act as a scattering factor.

Magnetic Properties of the ZnO−Spinel Film. Magnetic hysteresis measured at 298 K for the ZnO−spinel film is shown in Figure 9, showing that the film has a ferromagnetic behavior with magnetization of 34.2 emu cm^{-3} at a magnetic field of 5 kOe and coercive force of 172.5 Oe. The magnetic moment of Fe in the film was estimated to be 0.49 μ_B/Fe from the magnetization, and the temperature dependence of magnetization under a magnetic field of 1 kOe led to the Curie temperature of about 600 K as already reported.[8] The value of the magnetic moment was lower than that of bulk $Zn_{0.5}Fe_{2.5}O_4$, 1.92 μ_B/Fe.[19] Furthermore, a slightly increasing magnetic moment without saturation with increasing magnetic field above 2 kOe was also seen. Such superparamagnetic behavior at room temperature is a common phenomenon for magnetic particles smaller than 20 nm. These results

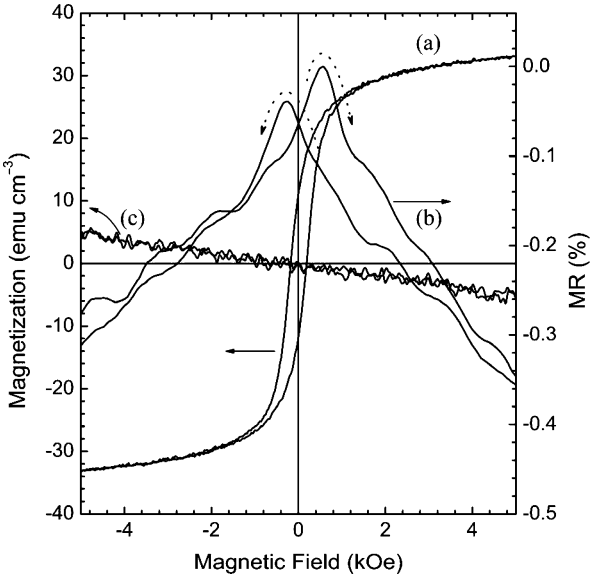

Figure 9. (a) Magnetization and (b) MR curves measured at 298 K for the ZnO−spinel film prepared on a glass substrate. (c) Magnetization curve for the ZnO film prepared on a glass substrate. The magnetic field was applied parallel to the film plane, and diamagnetic contribution from the glass substrate was subtracted. Dotted arrows indicate the sweeping direction of the magnetic field applied in the MR measurement.

suggest that the film contains much smaller spinel iron oxide particles exhibiting the nanosize effects, i.e., (i) the decrease of magnetic moment and (ii) superparamagnetic behavior,[16b,c,20] in addition to 20 nm particles with magnetic coercive force. The magnetic curve for the ZnO film containing no Fe is depicted for reference, showing diamagnetic behavior with no hysteresis.

The magnetic field dependence of the magnetoresistance ratio, MR (%), is defined as

$$\text{MR (\%)} = (\rho_H - \rho_{MAX})/\rho_{MAX} \quad (1)$$

where, ρ_H is electric resistivity at a certain magnetic field of H and ρ_{MAX} is its maximum value. Figure 9, curve b, shows MR measured at 298 K. The ZnO−spinel film showed a negative MR of about −0.35% at a magnetic field of 5 kOe (1 kOe = 0.1 T). The MR curve had two maxima around the magnetic fields corresponding to the coercive force of the magnetic hysteresis curve. For semiconductor−ferromagnet systems with a heterogranular structure, few have been reported to show a negative MR effect at room temperature, for instance, ZnO−Co[5] (ca. −0.13% in 5 kOe) and GaMnAs−MnAs[4l] (ca. −1% in 100 kOe). The origin of the negative MR in these systems is probably due to spin-dependent scattering of electrons.[21] The observation of the negative MR effect for the heterogranular film composed of spinel iron oxide particles embedded in semiconductor matrix as well as for the transparent ferromagnet film is reported here for the first time to the best of our knowledge. The detailed mechanism of the negative MR and an MR effect in the presence of large amounts of photoelectrons generated

(19) Smit, J.; Wijn, H. P. J. *Ferrites*; Wiley: New York, 1959; Chapter VIII.
(20) Goya, G. F.; Berquó, T. S.; Fonseca, C. F.; Morales, M. P. *J. Appl. Phys.* **2003**, *94*, 3520.
(21) Levy, P. M. *Solid State Phys.* **1994**, *47*, 367.

from the ZnO matrix by irradiation of UV light are under investigation.

Conclusions

A transparent ferromagnetic ZnO−spinel film with a heterogranular structure was prepared by chemical bath deposition in aqueous solutions and then by heat treatment at 773 k for 1 h. The resulting films were examined especially in terms of micro- and electronic structures by using TEM, XAFS, and SXMCD measurements. TEM observation revealed spinel iron oxide particles of about 20 nm in diameter dispersed in the ZnO matrix. XAFS and SXMCD studies at the Fe and Zn K-, $L_{2,3}$-edges using synchrotron radiation revealed consistently that the spinel iron oxide particles were Zn-substituted Fe_3O_4, $Zn_xFe_{3-x}O_4$ ($x \approx 0.5$), which caused the ferromagnetism. The ZnO−spinel film exhibited ferromagnetic behavior and negative MR effect as well as high transparency in the visible light regions and n-type semiconductivity, i.e., it was a transparent ferromagnetic semiconducting composite film. The results demonstrated in this study confirm the high potential of the chemical deposition method for preparing smart materials hybridized of semiconducting oxide and ferromagnetic oxide. Since the chemical process can be applied to highly resistive materials including p-type semiconductors, a new door for developing smart devices with a correlation among light, carrier, and spin can be opened.

Acknowledgment. XAFS and SXMCD measurements have been performed with the approval of SPring-8 (Proposal no. 2004A0201-NXa-np, 2004A0184-NSc-np, and 2005A0231-NXa-np). The authors thank Dr. T. Uruga, Dr. T. Nakamura, Dr. M. Takahashi, Dr. S. Watase, Dr. Y. Kobayashi, Dr. M. Watanabe, Mr. K. Mizuno and Mr. H. Aritomo for their kind help in the XAFS and SXMCD measurements. Kojundo Chemical Lab Co., Ltd. is acknowledged for supplying high-purity reagents.

CM052309T